Flux-line-lattice stability and dynamics

H. R. Glyde*
Department of Physics, University of Alberta, Edmonton, Alberta, Canada T6G 2J1

L. K. Moleko
Department of Physics, National University of Lesotho, P.O. Box 180, Lesotho, Africa

P. Findeisen
Department of Physics, University of Alberta, Edmonton, Alberta, Canada T6G 2J1
(Received 16 July 1991)

The mechanical stability of a flux-line lattice (FLL) having parameters appropriate for the high-T_c superconductors is determined using the self-consistent phonon theory of lattice dynamics. Nearly parallel flux lines (FL's) are assumed and FL pinning is neglected. The FLL becomes unstable when a phonon frequency goes to zero. At instability the rms vibrational amplitude diverges and the FL's can no longer be localized. In $Bi_2Sr_2CaCuO_2O_8$, the instability line as a function of temperature and magnetic field lies below but in reasonable agreement with the observed irreversibility line. In $YBa_2Cu_3O_7$, it lies significantly below. The present instability line is a reliable upper bound to the FLL melting line. Identifying instability with melting, we find the Lindemann criterion of melting does not hold. However, the present instability lines and the melting lines obtained by Houghton *et al.* are found to have similar shape.

I. INTRODUCTION

Flux lines (FL's) in high-temperature superconductors (HTSC's) display interesting dynamic,[1-6] entangled, and glassy[11-16] behavior. Since T_c is high, the FL's acquire significant thermal energy in the superconducting phase. The HTSC's are extreme type-II superconductors having a large Ginsburg-Landau ratio $\kappa=\lambda/\xi$. This means the correlation length ξ is small and that the interaction between the FL's is quite well represented by the weak magnetic repulsion described by the London field equations. The HTSC's are also extremely anisotropic, having a nearly layered structure. This layered structure may be represented by an anisotropic effective mass. The weak interaction combined with an anisotropic mass leads to large thermal displacements of the FL's below T_c and to interesting dynamic behavior.

To date, the HTSC's have been divided into "clean" and "dirty" materials. In clean materials pinning of FL's by impurities and defects is neglected and the flux lines form an ordered triangular lattice at low temperature.[7-10] Since T_c is high, this three-dimensional (3D) flux-line lattice (FLL) melts as a result of thermal vibration well below T_c. The melting temperature T_m is sensitive to κ and the anisotropic mass. Above T_m hexatic and entangled FL phases have been proposed.[8,14] In dirty materials, where pinning is dominant, the FL's form a glass[11-13] at low T. This glass also "melts" well[11-13,17] below T_c. Understanding this melting or depinning[5,6,18-21] is a critical issue in high-T_c superconducting technology since, if the FL's are mobile, there is energy loss in the superconducting state.

We study the lattice dynamics and mechanical stability of the FLL in clean HTSC's, ignoring pinning interactions. We make the approximation of nearly straight FL's. Specifically, with the FL's aligned along the z axis, we assume that $dr(z)/dz$ is small, where $r(z)$ $[r=(x,y)]$ is the position of the FL in the x-y plane at height z. The displacements of the FL's from their lattice points can be large, but the displacements are assumed to be smoothly varying with height z. The phonon frequencies and elastic constants are calculated using the FL interaction in this approximation proposed by Brandt.[22] Since phonon frequencies throughout the Brillouin zone are evaluated, the dispersive nature of the interaction is fully incorporated. Parameters appropriate to $Bi_2Sr_2CaCu_2o_8$ (Bi-Sr-Ca-Cu-O),[23] $YBa_2Cu_3O_7$ (Y-Ba-Cu-O),[24] and conventional superconductors are considered (see Table I).

For Bi-Sr-Ca-Cu-O we find that the rms vibrational amplitudes $\langle u^2\rangle^{1/2}$ are large with a typical Lindemann[25] ratio $\gamma=\langle u^2\rangle^{1/2}/a_0=0.25$, where a_0 is the triangular lattice spacing. The FLL is mechanically unstable well below T_c. At the instability temperature T_I, the transverse phonon frequencies go to zero and $\gamma\rightarrow\infty$. The phonon frequencies go to zero over a narrow temperature range characteristic of a sharp transition. Above the transition the FL's are no longer localized and the FL's can "pass through" each other, much as in the disentanglement models of mobility.[14] The instability line $T_I(B)$ lies below but in reasonable agreement with the observed[2] reversibility (FL mobility) lines in Bi-Sr-Ca-Cu-O. $T_I(B)$ lies farther below the reversibility line in Y-Ba-Cu-O. However, the values for the upper critical field $B_{c2}(T)$ used here are too low.

Below T_I the FLL is very harmonic and the anharmonic nature is important only near instability. We find that the Lindemann ratio γ is not constant along the $T_I(B)$ line; i.e., the Lindemann criterion[25] that γ is con-

stant at melting does not hold. However, the shape of the melting line obtained by Houghton, Pelcovits, and Sudbø[9] using the Lindemann criterion is similar to that found here. The present model and instability should provide an upper bound to melting of the FLL.

In Sec. II we set out the model for the 3D FLL and sketch the self-consistent phonon theory used to evaluate the FLL dynamics. Results for the phonon dispersion curves and the mechanical instability are presented in Sec. III. Elastic properties are set out in Sec. IV. The results are discussed in Sec. V.

II. FLUX-LINE LATTICE AND MODEL

A. Flux-line lattice

We consider N nearly straight, parallel FL's in a bulk HTSC sample. We assume that the applied field **B**, parallel to the c axis, penetrates the sample completely. The sample has length L (parallel to c, the z axis) and area A in the x-y plane (see Fig. 1). The total flux BA in the sample is confined to the N FL's, each line having a quantum of flux $\Phi_0=h/2e=2.07\times10^{-15}$ T m^2, $BA=N\Phi_0$. This requires a FL density $n=N/A=B/\Phi_0$. We assume a triangular FLL (see Fig. 1). The side of the triangle (lattice constant) a_0 is given by $A/N=n^{-1}=(\sqrt{3}/2)a_0^2$ or

$$a_0=\left[\frac{4}{3}\right]^{1/2}\left[\frac{\Phi_0}{B}\right]^{1/2} . \tag{1}$$

For a typical field, $B=2.65$ T$=26.5$ kG, $a_0=300$ Å.

The magnetic flux associated with each FL penetrates a distance $\lambda\approx3000$ Å into the superconducting region around the FL. There is magnetic energy stored in this field. This leads to a "self-energy" of each line and to a repulsive "interaction" energy between lines resulting from the overlap of the magnetic fields of neighboring lines. These magnetic energies may be evaluated using London's field equations.[22,26] For nearly straight, parallel lines, the interaction potential is[22]

$$U_2=\frac{1}{2}\sum_{i,j}{}' V(r_{ij})=\frac{V_0}{2}\sum_{i,j}{}' v(r_{ij}) , \tag{2}$$

where $V_0=\Phi_0^2/2\pi\lambda^2\mu_0$,

$$v(r)=K_0\left[\frac{r}{\lambda'}\right]-K_0\left[\frac{r}{\xi'}\right] , \tag{3}$$

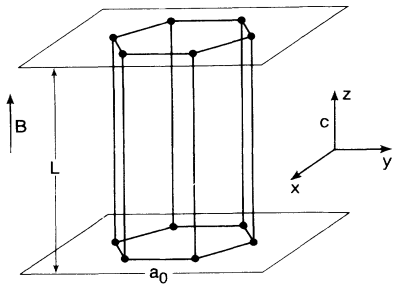

FIG. 1. Triangular flux-line lattice.

and

$$\lambda'=\lambda(T)/(1-b)^{1/2},\quad \xi'=\xi/[2(1-b)]^{1/2} . \tag{4}$$

The coefficient V_0 sets the interaction energy per unit length of the FL's where $\mu_0=4\pi\times10^{-7}$ W/(A m) is the permeability of free space ($T=$W/m^2). The first repulsive term in (3), $K_0(r/\lambda')$, comes from the magnetic energy.[26] In (3), $K_0(x)$ is a modified Bessel function having asymptotic values

$$K_0(x)\sim\begin{cases}\left[\dfrac{\pi}{2x}\right]^{1/2}e^{-x} & \text{as } x\to\infty ,\\ -\ln(x/2)-0.577 & \text{as } x\to0 .\end{cases} \tag{5}$$

λ' is the field-dependent penetration depth [$b=B/B_{c2}(T)$], where $B_{c2}(T)=B_{c2}(1-t)$ is the upper critical field, $\lambda(T)=\lambda/(1-t^4)$, and $t=T/T_c$. $\xi^2=\Phi_0/2\pi B_{c2}$ is the FL correlation length $\lambda=\kappa\xi$.

The second attractive term $K_0(r/\xi')$ ensures that $v(r)$ is finite when the FL cores overlap ($r<\xi'$). Brandt[22] obtained (2) from his general potential for arbitrarily shaped FL's by assuming nearly straight lines. For Bi-Sr-Ca-Cu-0 we have used $B_{c2}=44$ T, which is probably too small. This gives a correlation length

$$\xi=\left[\frac{\Phi_0}{2\pi B_{c2}}\right]^{1/2}\simeq30 \text{ Å} . \tag{6}$$

We have used $\kappa=\lambda/\xi=95$. Thus, in Bi-Sr-Ca-Cu-O, we have here

$$\lambda\sim10a_0\sim100\xi . \tag{7}$$

In this case the magnetic field of one FL overlaps many neighbors, $\lambda\gtrsim10a_0$, but the cores of the FL's are well separated, $\xi\sim a_0/10$. The interaction is very long range (see Fig. 2), and in the sum in (2) we have typically summed over 30 000 shells of FL's.

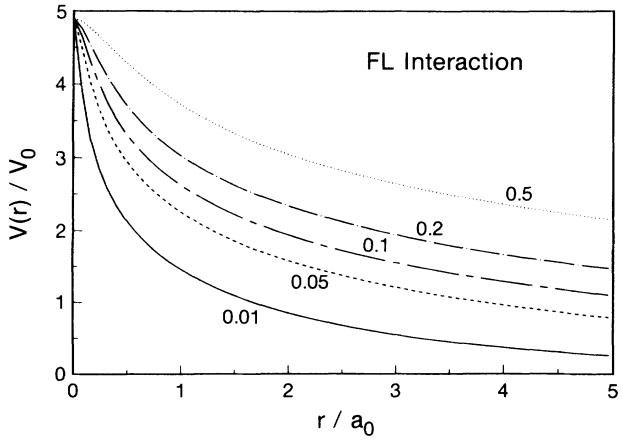

FIG. 2. Flux line pair potential $V(r)/V_0=K_0(r/\lambda')-K_0(r/\xi')$ given by (3) for $0.01\le b\le0.5$ using parameters appropriate for Bi-Sr-Ca-Cu-O: $B_{c2}=44$ T, $\xi^2=\Phi_0/(2\pi B_{c2})$, $\lambda=\kappa\xi$, $\kappa=95$, $\xi'=\xi/[2(1-b)]^{1/2}$, $\lambda'=\lambda/(1-b)^{1/2}$, $b=B/B_{c2}$, and lattice spacing $a_0^2=(\frac{4}{3})^{1/2}(\Phi_0/B)$.

The elastic or self-energy of a FL, ε_1, may be obtained from (2) and (3) by setting $r=0$. This gives

$$\varepsilon_1 = V_0 \ln\kappa \ , \tag{8}$$

which represents the stored magnetic energy per unit length. If the end points of the FL are fixed and we displace the FL at its midpoint in the x-y plane, the FL length is increased. The energy associated with the increased length δl is $\delta E=\varepsilon_1 \delta l$. For anisotropic materials a closer analysis[8] shows that for displacements in the x-y plane, ε_1 should be replaced by

$$\tilde{\varepsilon}_1 = \frac{\varepsilon_1}{M_z/M} = \left[\frac{\Phi_0^2}{2\pi\lambda^2\mu_0}\right]\frac{\ln\kappa}{M_z/M} \ , \tag{9}$$

where M_z and M are the effective mass parallel and perpendicular to the c axis.

Taking account of the self- and interaction energies, the free energy of the FLL for an arbitrary location $r_i(z)$ of the FL's is[8]

$$\frac{F}{kT} = \frac{1}{kT}\int_0^L dz \left[\frac{1}{2}\tilde{\varepsilon}_1 \sum_i \left(\frac{dr_i}{dz}\right)^2 + \frac{1}{2}\sum_{i,j}{}' V(r_i(z)-r_j(z))\right] . \tag{10}$$

The first term is the stretching self-energy valid for displacements $r_i(z)$ slowly varying with z, i.e., dr_i/dz small. The FL's, however, can be displaced a large distance from their lattice points. The interaction is "local" in z in the sense that interaction between FL's at the same height z only is accounted for in (10). The local and $dr_i/dz \ll 1$ limits are valid for nearly straight FL's.

B. Boson analogy

The free energy F/kT in (10) can be used to calculate the classical partition function (configuration integral) for the 3D FLL. A monolayer of bosons confined to the x-y plane can be described by the action

$$S = \frac{1}{\hbar}\int_0^{\beta\hbar} d\tau \left[\frac{1}{2}M_B \sum_i \left(\frac{dr_i}{d\tau}\right)^2 + \frac{1}{2}\sum_{i,j}{}' V_B(r_i(\tau)-r_j(\tau))\right] . \tag{11}$$

This action S may be used to evaluate the partition function of the bosons in a path-integral representation. Nelson and Seung[8] have emphasized that the 3D FLL and the monolayer of bosons are identical (have identical partition functions) if we set

$$M_B = \left[\frac{\hbar}{kT}\right]\tilde{\varepsilon}_1, \quad V_B = \left[\frac{\hbar}{kT}\right]V \ , \tag{12}$$

where $\tilde{\varepsilon}_1$ and V are given by (9) and (2), respectively. Thus we may "map" the 3D FLL onto a monolayer of bosons. We have also taken $L\to\infty$ so that $\beta\hbar\to\infty$. Thus the classical 3D FLL (at temperature T) having infinite height corresponds to a monolayer of bosons at $T=0$ K. We have used this boson analogy to evaluate the lattice dynamics of a monolayer of bosons having mass M_B interacting via potential V_B and translated this back to the 3D FLL using (12). The boson interaction in (11) is local in time.

C. Self-consistent phonons

The self-consistent theory of lattice dynamics for 2D systems has been discussed extensively.[27] We sketch here only the self-consistent harmonic (SCH) approximation. In the SCH approximation, the frequency $\omega_{q\lambda}$ of a phonon having wave vector $\mathbf{q}$ and branch λ is given by the usual harmonic result

$$\omega^2_{\mathbf{q}\lambda} = \frac{1}{M_B}\sum_{\alpha,\beta}^{2} \epsilon_\alpha(\mathbf{q},\lambda)\epsilon_\beta(\mathbf{q},\lambda)\sum_j{}' (1-e^{-i\mathbf{q}\cdot\mathbf{R}_{ij}})\Phi_{\alpha\beta}(i,j) \ , \tag{13}$$

where $\epsilon(\mathbf{q},\lambda)$ are the polarization vectors and R_j are the triangular lattice vectors. The SCH force constants $\Phi_{\alpha\beta}$ are the usual second derivative of the potential V_B averaged over the vibrational displacements $u_i=r_i-R_i$ of the FL's from the lattice points, i.e.,

$$\Phi_{\alpha\beta}(i,j) = \left\langle \frac{\partial^2 V_B(r_{ij})}{\partial u_\alpha \partial u_\beta}\right\rangle , \tag{14}$$

where $u=u_{ij}=u_i-u_j$ is the relative displacement. The dependence of $\Phi_{\alpha\beta}$ on the vibrational displacements is a key feature of the SCH approximation. We assume a Gaussian vibrational distribution

$$\langle\ \rangle = (2\pi^2|\underline{\Lambda}|)^{-1/2}\int d\mathbf{u}\, e^{-(1/2)\mathbf{u}\cdot\underline{\Delta}^{-1}\cdot\mathbf{u}} \ , \tag{15}$$

having width given by

$$\Lambda_{\alpha\beta}(i,j) = \langle (u_i-u_j)_\alpha (u_i-u_j)_\beta\rangle = \frac{\hbar}{NM_B}\sum_{\mathbf{q},\lambda}(1-e^{i\mathbf{q}\cdot\mathbf{R}_{ij}})\epsilon_\alpha(\mathbf{q},\lambda)\epsilon_\beta(\mathbf{q},\lambda)\frac{1}{\omega_{q\lambda}} \ . \tag{16}$$

Equations (13)–(16) constitute the SCH approximation. The equations are iterated until consistent. Except near the instability (large B or large T), we found that the FLL was very harmonic. This means that, although $\Lambda_\alpha(i,j)$ may be large, the Gaussian in (15) is well approximated by a delta function $\delta(u_{ij})$. This is because the potential $V(r)$ is slowly varying with r.

The $V(r)$ for different fields B is shown in Fig. 2. As $b=B/B_{c2}$ increases, the potential becomes flatter and of larger range. At a critical B and T, the $V(r)$ is so flat that the FL's can no longer be confined by $V(r)$. In this case the rms vibrational amplitude continues to increase in the iterations of the SCH equations. At instability, adjacent flux lines can pass through one another (parallel flux-line cutting).

The Lindemann ratio $\gamma^2=\langle u_i^2\rangle/a_0^2$ may be calculated directly from the $\omega_{q\lambda}$ as

$$\gamma^2=\frac{\langle u_i^2\rangle}{a_0^2}=\frac{1}{a_0^2 N}\sum_{q,\lambda}\left[\frac{\hbar}{2M_B\omega_{q\lambda}}\right] \tag{17}$$

$$=\frac{kT}{Na_0^2}\sum_{q,\lambda}\left[\frac{1}{2\bar{\epsilon}_1\omega_{q\lambda}}\right]. \tag{18}$$

Equation (17) is the $T=0$ K boson result, and in (18) we have used (12). Indeed, the boson analogy can be developed by requiring that γ be the same for the bosons at $T=0$ K and for the FLL at temperature T. Equation (18) can be reduced to the approximate result quoted by Nelson and Sueng,[8]

$$\gamma^2=\frac{kT}{a_0^2}\left[\frac{n}{4\pi K\mu}\right], \tag{19}$$

by retaining only the long-wave limit of the transverse phonon frequencies, where $\mu=c_{66}=(V_0 n/16)2$ is an approximate transverse elastic constant, and allowing $\bar{\epsilon}_1 n$ to play the role of the tilt modulus, $K=c_{44}=\bar{\epsilon}_1 n$, where $n=B/\Phi_0$. We have found that (18) and (19) give comparable values for γ at low T and B.

III. PHONONS AND MECHANICAL STABILITY

The SCH phonon frequencies $\omega_{q\lambda}$ describing the collective vibrations of the FLL in the x-y plane are shown in Fig. 3 for Bi-Sr-Ca-Cu-O at $T=15$ K in applied field $B=2.65$ T. The parameters characterizing Bi-Sr-Ca-Cu-O are listed in Table I. The "boson mass" is $M_B=\hbar\bar{\epsilon}_1/kT\sim(M_z/M)^{-1}$, so that a large anisotropy corresponds to a "light" FL and to large-amplitude vibration. In Fig. 3 the dispersion curves run from the center of the Brillouin zone (BZ) Γ to the BZ edge K, along the BZ edge from K to M and back to the BZ center. The longitudinal (L) frequencies lie well above the transverse (T) values, reflecting the large anisotropy of the FLL; i.e., the longitudinal elastic constant is $\lambda\approx c_{66}\sim 5\times 10^3\mu$. $\omega_{q\lambda}^2$ may be viewed as diagonal, q-dependent elastic constants. At $T=15$ K the SCH and harmonic (H) frequencies are identical and the Lindemann ratio is $\gamma=0.20$. This shows that even for large γ the FLL dynamics is harmonic, which follows from the smooth potential shown in Fig. 2. We have also evaluated the cubic anharmonic contribution to $\omega_{q\lambda}$ and found it negligible.

TABLE I. Parameters used to represent Bi-Sr-Ca-Cu-O and Y-Ba-Cu-O (see Refs. 9, 23, and 24).

	T_c (K)	B_{c2} (T)	κ	M_z/M
Bi-Sr-Ca-Cu-O	87	44	95	3600
Y-Ba-Cu-O	87	44	50	25

In Fig. 4 we show $\gamma(T)$ at $B=2.65$ T ($a_0=300$ Å, $\lambda\simeq 3000$ Å) calculated in the harmonic approximation from (18) in Bi-Sr-Ca-Cu-O as a function of T. There we see $\gamma(T)$ is large. In the harmonic approximation (HA) for purely T-independent parameters, $\gamma(T)$ is proportional to $\sqrt{T}$. There is significant departure from $\sqrt{T}$ at higher T since $B_{c2}(T)$ and $\lambda'(T)$ depend on T. At $T\approx 62$ K, $\gamma(T)$ diverges, reflecting the temperature at which the harmonic transverse elastic constant $\mu_H\to 0$.

In Fig. 5 we show the SCH frequencies in Bi-Sr-Ca-Cu-O for $B=2.65$ T and $T=22$ K right on the instability line. Shown are $\omega_{q\lambda}$ from four consecutive iterations (1,2,3,4) of the SCH equations. Iteration one (1) is the harmonic limit. In successive iterations the $\omega_{q\lambda}$ decrease until on the fourth iteration most of the transverse frequencies ω_{qT} have become imaginary [$\omega_{q\lambda}^2$ in (13) becomes negative]. At this B and T, the FLL is unstable to vibration. The corresponding Lindemann ratio calculated from (17) diverges, and the FL's can no longer be localized. We have found that instability is sudden, occurring over a narrow range of T and B. Right up to the instability, the dynamics is very harmonic. At instability the interaction potential is not steep enough to confine the FL's at their lattice points.

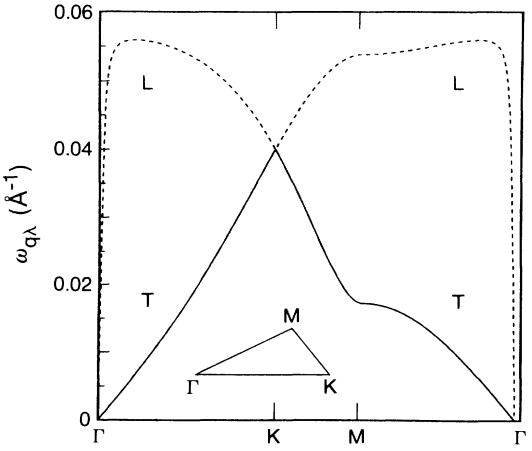

FIG. 3. SCH phonon frequency dispersion curves in Bi-Sr-Ca-Cu-O at $T=15$ K and $B=2.65$ T. Γ is the Brillouin-zone center, and points K and M are at the zone edge. The $\omega_{q\lambda}$ are in (length)$^{-1}$, the units in the corresponding boson model.

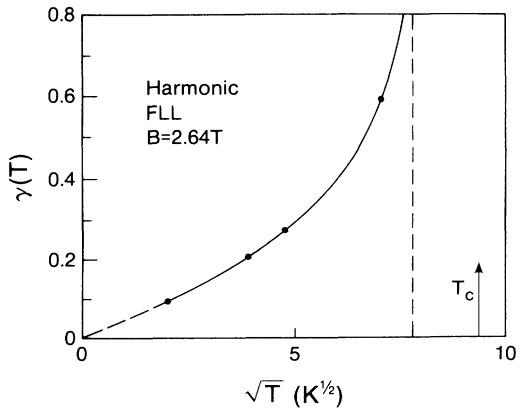

FIG. 4. Lindemann ratio $\gamma=\langle u^2\rangle^{1/2}/a_0$ in Bi-Sr-Ca-Cu-O in the harmonic approximation (HA). In the HA with T-independent parameters, $\gamma\propto\sqrt{T}$. The vertical dashed line indicates T_l in the HA where γ diverges.

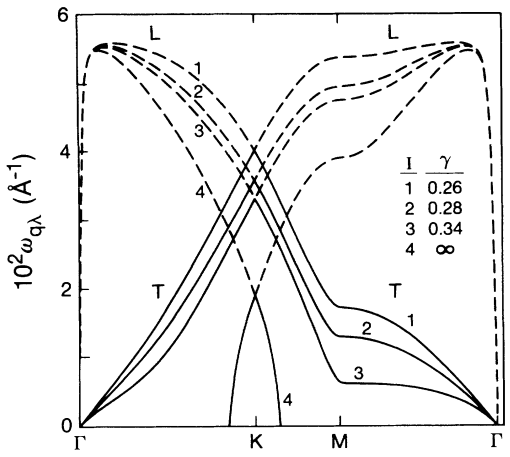

FIG. 5. Self-consistent harmonic (SCH) dispersion curves in Bi-Sr-Ca-Cu-O at $T=22$ K and $B=2.65$ T, showing FLL instability. As Eqs. (13), (14), and (16) are iterated, the transverse (T) frequencies decrease in value in successive iterations (1,2,3,4) until on iteration 4 the $\omega_{qT}\rightarrow 0$. The corresponding γ given by (18) in each iteration is listed.

The FLL instability line in Bi-Sr-Ca-Cu-O obtained here in the SCH approximation is shown in Fig. 6 as a solid line with squares. The numbers on the line are the Lindemann ratio just below instability. We see that the Lindemann ratio is not constant at instability, varying from 0.17 to 0.30 in the range shown. The SCH instability line lies well below $B_{c2}(T)$ and below the irreversibility line observed by Gammel *et al.*[12] The solid line with diamonds shows a melting line calculated by Ma and Chui[28] using the same parameters as in Table I for Bi-Sr-Ca-Cu-O. This is a Monte Carlo calculation which uses the same potential (1), but does not make the approximation of nearly straight FL's or the SCH approximation. We expect the present instability to be an upper bound to

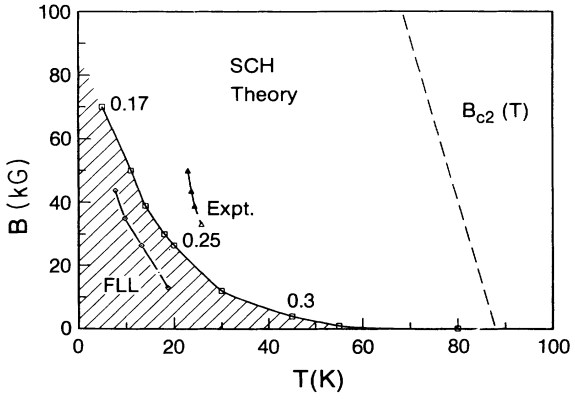

FIG. 6. FLL instability line in Bi-Sr-Ca-Cu-O ($B_{c2}=44$ T, $\kappa=95$, $M_z/M=3600$, and $T_c=87$ K) calculated here in the SCH approximation (solid line with squares). The solid line with diamonds is the FLL melting line calculated by Ma and Chui (Ref. 28) without assuming nearly straight FL's. The solid line with triangles is the observed reversibility line identified with the onset of free motion of the FL's (Ref. 2). The numbers are the Lindemann ratio γ immediately below the instability.

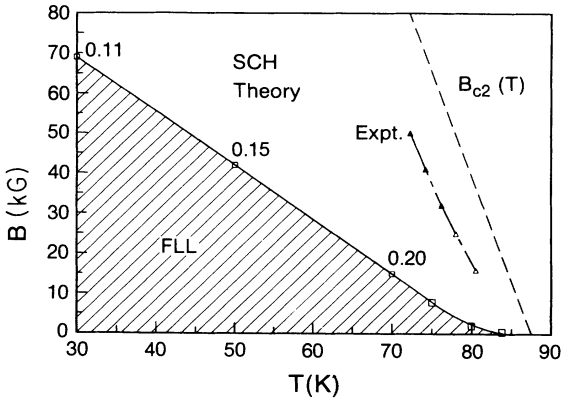

FIG. 7. As in Fig. 6 for Y-Ba-Cu-O ($B_{c2}=44$ T, $\kappa=50$, $M_z/M=25$, and $T_c=87$ K).

melting; i.e., the lattice might melt for thermodynamic reasons before it becomes mechanically unstable. Also, the SCH approximation itself gives an upper limit to instability.[29] We believe this is a close limit for the present potential since higher anharmonic terms make a negligible contribution. Assuming nearly straight FL's leads to a stiffer and more stable FLL. For all these reasons, the present instability is an upper bound to the FLL melting line. Comparison with Ma and Chui[28] suggests that the present upper bound is reasonably close to the actual melting line.

From Fig. 6 we see that the calculated instability or melting line lies below experiment. This could be due to the low value of B_{cz} used here. A higher B_{c2} would scale the instability to higher B. Or it may be that the observed reversibility is not associated with melting, but rather with depinning in the FL liquid.[5,6,18]

In Fig. 7 we show the instability line in Y-Ba-Cu-O. Again, we see that the Lindemann ratio is not constant at instability. In Y-Ba-Cu-O, $\gamma(T,B)$ is significantly smaller because the boson mass (M/M_z) is larger in Y-Ba-Cu-O. The smaller γ apparently leads to a nearly straight melting line. In Y-Ba-Cu-O the instability line lies ~ 25 K below the observed reversibility line at $B\sim 5$ T. This difference is ~ 10 K in Bi-Sr-Ca-Cu-O.

IV. ELASTIC CONSTANTS

The elastic constants in the SCH approximation may be calculated from the long-wave limit of the SCH dispersion curves shown in Figs. 3 and 5. From the dispersion curves in Fig. 5, we see that the transverse frequencies at low Q vanish at the instability. Thus the corresponding transverse elastic constant $\mu=c_{66}$ vanishes at the instability in the SCH approximation.

We have found that μ also vanishes in the HA, but at a higher temperature than in the SCH case. In the HA, μ is[22]

$$\mu_H=\left[\frac{V_0 n}{16}\right]\sum_i\left[R_i^2 v''(R_i)+3R_i v'(R_i)\right]. \tag{20}$$

By direct evaluation of this sum, $\mu(T,B)$ can be calculated in the present model. As a check we confirmed that

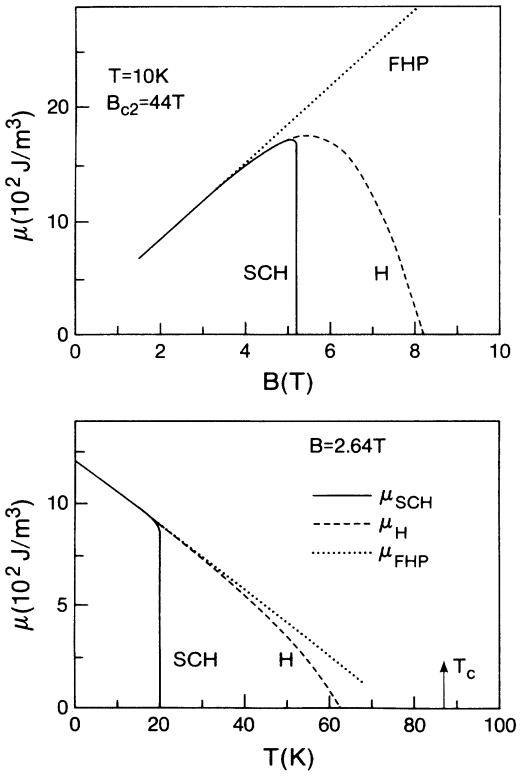

FIG. 8. Transverse elastic constant $\mu=c_{66}$ of the FLL in Bi-Sr-Ca-Cu-O in the self-consistent harmonic (SCH) and harmonic (H) approximations. Also shown in μ_{FHP}, the Fetter, Hohenberg, and Pincus (Ref. 30) expression $\mu=(n\Phi_0^2/2\pi\lambda'^2\mu_0)/8$, where $n=B/\Phi_0$. The upper figure shows μ at constant T vs B and the lower figure μ at constant B vs T.

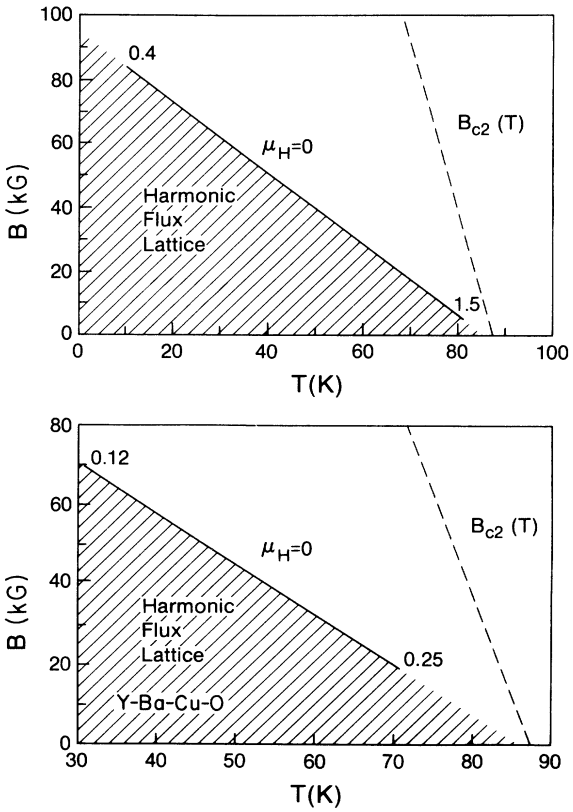

FIG. 9. Instability of the FLL in the harmonic approximation identified by vanishing of the harmonic transverse elastic constant $\mu=c_{66}$. The upper-figure is Bi-Sr-Ca-Cu-O and the lower figure is Y-Ba-Cu-O.

the direct evaluation of (20) agreed with $\mu_H(T,B)$ evaluated from the long-wave limit of the harmonic ω_{qT}. In Fig. 8 we show $\mu(10\text{ K},B)$ and μ at constant $B=2.65$ T vs T, $\mu(T,265\text{T})$ in the SCH and H approximations. For comparison we have plotted μ derived by Fetter, Hohenberg, and Pincus,[30]

$$\mu_{FHP}=\left[\frac{V_0 n}{16}\right]2 = \left[\frac{\Phi_0 B_{c2}(T)}{2\pi\lambda^2\mu_0 16}\right]2b(1-b)\ , \tag{21}$$

where $B_{c2}(T)=B_{c2}(0)(1-t)$ and $b=B/B_{c2}$. Clearly, (20) and (21) agree well at low T and low B. The temperature dependence of μ_{FHP} comes predominantly from $B_{c2}(T)$ and less so from $\lambda(T)$. From Fig. 8 we see that μ_H in (20) vanishes below T_c and below B_{c2}. The μ_{FHP} is finite essentially over the whole superconducting range. Thus the present model of nearly straight flux lines interacting via the interaction (2) predicts that the FLL is mechanically unstable ($\mu_H=0$) below T_c in the harmonic approximation. This instability occurs above the mechanical instability already predicted by the more complete SCH approximation and so is of academic interest only. The lines $\mu_H(T,B)=0$ for Bi-Sr-Ca-Cu-O and Y-Ba-Cu-O are set out in Fig. 9.

The longitudinal elastic constant λ ($c_{11}=\lambda+2\mu$) can also be calculated. This λ is typically 5×10^3 times greater than μ ($c_{11}\approx\lambda$), reflecting the large anisotropy. Direct evaluation of λ from $V(r)$ agreed well with

$$\frac{B^2}{2\mu_0}=\lambda+\mu\approx\lambda\ .$$

For example, we obtained $\lambda=5.54\times10^6$ J/m^3 at $B=2.64$ T and $T=22$ K. The λ is temperature independent except right near T_c, since the penetration length is $\lambda(T)=\lambda(0)(1-t^4)^{1/2}$.

Finally, we have evaluated the instability line for a "conventional" type-II superconductor, represented by $B_{c2}=4$ T, $K=3$, $M_z/M=1$, and $T_c=10$ K. In this case the Lindemann ratio is very small, $\gamma\sim0.005$. The FLL is unstable below but close to $B_{c2}(T)$ for this case. Since γ is so small, the FLL is very harmonic and the instability line in the SCH and the harmonic (H) approximations are identical. The present model is less appropriate for conventional superconductors since ξ and $\lambda=\kappa\xi$ are comparable.

V. DISCUSSION

The Lindemann ratio γ found here near the FLL instability is largest for Bi-Sr-Ca-Cu-O ($\gamma\simeq0.3$) and smallest

in the conventional superconductors ($\gamma \approx 0.01$). γ is a sensitive function of M_z/M and κ, particularly of M_z/M. If M_z/M is large, the stretching modulus $\bar{\epsilon}_1$ is small. This means that the FL can be displaced with little increase in energy and large vibrational amplitudes are possible. The corresponding boson mass $M_B=(\hbar/kT)\bar{\epsilon}_1$ is small, leading to a large kinetic energy and large values of $\langle u^2 \rangle$ in the boson model.

When γ is small the instability in the harmonic approximation, identified as the point where the harmonic transverse elastic constant $\mu_H(T,B)=0$, coincides or nearly coincides with the instability in the SCH approximation. This is the case for conventional superconductors and nearly so for Y-Ba-Cu-O (compare Figs. 7 and 9). For smaller γ and in the harmonic approximation, the instability line is nearly straight, e.g., Figs. 7 and 10. In Bi-Sr-Ca-Cu-O, γ is significantly larger. In this case the SCH instability line differs significantly from the harmonic result. The SCH instability line of Bi-Sr-Ca-Cu-O, shown in Fig. 6, is also curved. Thus the shape of the instability line appears to depend on γ (on M_z/M). The only difference between Bi-Sr-Ca-Cu-O and Y-Ba-Cu-O here are the values of M_z/M and κ.

We have found that the Lindemann ratio is not constant at instability. It differs by a factor of 2 in a given material, as T or B is varied, and differs by an order of magnitude from material to material, e.g., Bi-Sr-Ca-Cu-O to conventional superconductors. In other solids the Lindemann criterion of melting appears to hold in the classical limit. That is, for crystals melting at temperatures where quantum effects are negligible, melting takes place when $\gamma=0.16$, independent of the material.[31-34] A specific example is the Wigner crystal.[34] However, when melting takes place when quantum effects are important, γ is not constant. For example, in solid helium $\gamma=0.25-0.35$, in the Wigner crystal[35] at $T=0$ K, $\gamma \simeq 0.33$, and for the Gaussian core model, $0.04 \leq \gamma \leq 0.35$ at melting.[29] Thus it is not clear whether a Lindemann criterion is expected for the FLL and we do not find one here. In spite of this, it is interesting that Houghton, Pelcovits, and Sudbø[9] obtained melting curves in Bi-Sr-Ca-Cu-O and Y-Ba-Cu-O using the Lindemann criteria having shapes similar to those found here in Figs. 6 and 7. This needs further study. We have also investigated the square FLL and found that it was unstable ($\mu_H=0$) at all T and B.

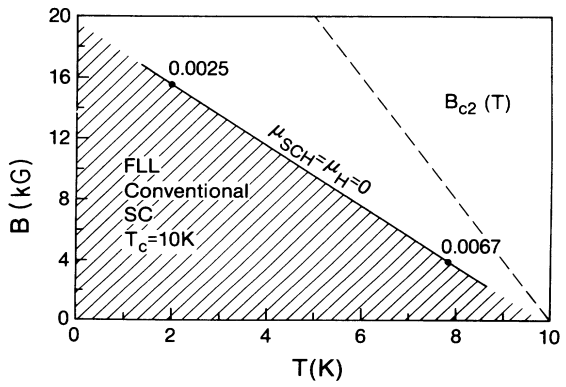

FIG. 10. Instability line in a conventional superconductor ($B_{c2}=4$ T, $\kappa=3$, $M_z/M_1=1$, and $T_c=10$ K). In this case the FLL is very nearly harmonic ($\gamma \lesssim 0.01$) and the SCH and H approximations are identical.

In the SCH approximation, we believe the instability takes place when the potential can no longer confine the FL's to lattice points. At instability the FL's can pass through each other. As seen from Fig. 2, the FL interaction does not have a "hard core" preventing overlap of the FL's. As T increases and $\langle u^2 \rangle$ increases, a critical temperature is reached when the FL can no longer be contained by the soft core potential and FL's can pass through one another. To check this point, we added a narrow hard core of height $V/V_0=10^3$ to $V(r)$ in Fig. 2. With the hard core, the instability temperature increased by more than a factor of 2 and the character of the instability changed significantly. We identify instability with FL's passing through each other much as in disentanglement models of melting.[14]

The upper critical field $B_{c2}=44$ T used here is too low.[36] Since the field B enters the present model as $b=B/B_{c2}$, increasing B_{c2} would scale our instability line to higher B values. Indeed, we have found that, at constant temperature, the field B at which instability takes place is directly proportional to B_{c2}. Only ξ in (6) depends on B_{c2} itself, and the instability is relatively insensitive to ξ. Once B_{c2} is known, this scaling can be made. This will bring our instability lines into better agreement with the observed irreversibility lines.

As noted, we have used a local interaction in (2) and (10). This means that interaction between FL's at the same height z only is considered. In a nonlocal interaction, interactions between FL's at different heights, $v(r_i(z_i)-r_j(z_j))$, are incorporated. If the FL's are nearly straight, the nonlocal expression reduces to the local result (2). Using a local interaction generally leads to stiffer elastic properties.[5,37] Thus the present instability is an upper limit to the nonlocal case. Instability is also an upper limit to melting. These points are consistent with the melting line obtained by Ma and Chui,[28] who used the corresponding nonlocal potential, lying somewhat below the present instability line as shown in Fig. 6. We emphasize that the boson analogy can be carried through for a nonlocal interaction. It leads to an interaction in (11), which is nonlocal in time, and to a more complicated kinetic energy, reflecting the anisotropy of the interaction. Path integrals with nonlocal interactions have proved useful in many instances. An important next step is to incorporate the nonlocal interaction[38] in the FLL dynamics.

We have also neglected pinning of FL's. The observed irreversibility line has been interpreted[39-42,37] as thermally activated depinning of FL's rather than melting. Other measurements[43,44] of the irreversibility line in single-crystal Y-Ba-Cu-O, often interpreted[37] as a depinning line, lie above but close to the line observed by Gammel *et al.*[2] shown here in Fig. 7. An important step would be to incorporate pinning of the FL's in the present model. Simulations[17] suggest that in the presence of pinning, the FLL melting line is depressed to lower temperature.

Civale, Worthington, and Gupta[45] have reported an interesting dependence of the irreversibility line with thick-

ness in Y-Ba-Cu-O films. As the thickness is reduced, the irreversibility line moves to lower temperature. This dependence can be understood within FLL melting and the boson model. Comparing (10) and (11), the FLL thickness L corresponds to $\hbar/kT$ in the boson model. A finite L, corresponds to a finite T; a smaller L corresponds to higher T in the boson model. Thus we would expect the FLL to melt more readily as L is reduced.

Thermal melting in crystals can generally be related to the Debye temperature or some other characteristic temperature, say, $T_m \sim \Theta_D$ ($T_m = \alpha\Theta_D$). In the boson model, $L \Longrightarrow \hbar/kT$ or $T_m \Longrightarrow (\hbar/k)L_m^{-1}$. The Debye temperature is $\Theta_D = \hbar\omega_D/k$. Thus we have

$$\alpha^{-1} = \frac{\Theta_D}{T_m} \Longrightarrow \omega_D L_m$$

or

$$L_m \Longrightarrow 1/\alpha\omega_D \ .$$

The characteristic ω_D in Y-Ba-Cu-O we find here is $\omega_D \simeq 0.005$ Å^{-1} or $L \sim 200$ Å with $\alpha = 1$. The observed decrease in the irreversibility line begins at $L \simeq 1000$ Å in Y-Ba-Cu-O, which is the same order. In Bi-Sr-Ca-Cu-O we find that $\omega_D \simeq 0.05$ Å^{-1} (see Figs. 3 and 5 where the maximum $\omega_{q\lambda} \simeq 0.055$ Å^{-1}). Thus, in Bi-Sr-Ca-Cu-O, this argument suggests that the onset of the thickness dependence of the irreversibility line due to "finite temperature melting in the boson model" will begin at $L \simeq 100$ Å. Thus, if irreversibility is partially related to FLL melting, there should be a significant difference in the onset of the thickness dependence of T_m between Y-Ba-Cu-O and Bi-Sr-Ca-Cu-O. FLL stability in films is the subject of a forthcoming paper.

In conclusion, we have obtained an instability limit for the FLL. This represents an upper limit to the FLL melting line. The instability line lies below the observed reversibility line in Bi-Sr-Ca-Cu-O and Y-Ba-Cu-O. One reason that the present instability line is too low is because we have used a low value of $B_{c2} = 44$ T. The present model depends on $b = B/B_{c2}$ and can be scaled to higher B when B_{c2} is known. Although we find that the Lindemann criterion does not hold, the shape of the "melting" lines obtained here is similar to that obtained by Houghton, Pelcovits, and Sudbø.

ACKNOWLEDGMENTS

It is a pleasure to acknowledge valuable discussions with S. T. Chui and NSERC, Canada, for support.

*Present address: Dept. of Physics and Astronomy, University of Delaware, Newark, DE 19711

[1]P. L. Gammel, D. J. Bishop, G. J. Dolan, J. R. Kwo, C. A. Murray, L. F. Schneemeyer, and J. V. Waszczak, Phys. Rev. Lett. **59**, 2592 (1987).
[2]P. L. Gammel, L. F. Schneemeyer, J. V. Waszczak, and D. J. Bishop, Phys. Rev. Lett. **61**, 1666 (1988).
[3]R. S. Markiewicsz, J. Phys. C **21**, L1173 (1988).
[4]E. Rodriguez, J. Luzuriaga, C. A. D'Ovidio, and D. A. Esparza, Phys. Rev. B **42**, 10 796 (1990).
[5]E. H. Brandt, Phys. Rev. Lett. **63**, 1106 (1989).
[6]E. H. Brandt, P. Esquinazi, and G. Wiess, Phys. Rev. Lett. **62**, 2330 (1989).
[7]D. R. Nelson, Phys. Rev. Lett. **60**, 1973 (1988).
[8]D. R. Nelson and H. S. Seung, Phys. Rev. B **39**, 9153 (1989).
[9]A. Houghton, R. A. Pelcovits, and A. Sudbø, Phys. Rev. B **40**, 6763 (1989).
[10]M. A. Moore, Phys. Rev. B **39**, 136 (1989).
[11]S. John and T. C. Lubensky, Phys. Rev. B **34**, 4815 (1986).
[12]M.P.A. Fisher, Phys. Rev. Lett. **62**, 1415 (1989).
[13]D. Fisher, M.P.A. Fisher, and D. Huse, Phys. Rev. B **43**, 130 (1991).
[14]S. Obukhov and M. Rubinstein, Phys. Rev. Lett. **65**, 1279 (1990).
[15]D. R. Nelson and P. Le Doussal, Phys. Rev. B **42**, 10 113 (1990).
[16]M. C. Marchetti and D. R. Nelson, Phys. Rev. B **41**, 1910 (1990).
[17]H. J. Jensen, A. Brass, A-C Shi, and A. J. Berlinsky, Phys. Rev. B **41**, 6394 (1990), and references cited therein.
[18]M. Tinkham, Phys. Rev. Lett. **61**, 1658 (1988).
[19]D. Feinberg and C. Villard, Phys. Rev. Lett. **65**, 919 (1990).
[20]J. R. Clem and M. W. Coffey, Phys. Rev. B **42**, 6209 (1990).
[21]H. Svensmark and L. M. Falicov, Phys. Rev. **42**, 9957 (1990).
[22]E. H. Brandt, Phys. Rev. B **34**, 6514 (1986).
[23]T.T.M. Palstra, B. Batlogg, L. F. Schneemeyer, R. B. van Dover, and J. V. Waszczak, Phys. Rev. B **38**, 5102 (1988).
[24]Y. Iye, T. Tanegai, H. Taeya, and H. Takei, Physica B **148**, 224 (1987).
[25]F. Lindemann, Phys. Z. **11**, 609 (1910).
[26]M. Tinkham, *Introduction to Superconductivity* (McGraw-Hill, New York, 1975), Chap. 5.
[27]T. M. Hakim and H. R. Glyde, Phys. Rev. B **41**, 1640 (1990); T. M. Hakim, H. R. Glyde, and S. T. Chui, *ibid.* **37**, 974 (1988); L. K. Moleko, B. Joos, T. M. Hakim, H. R. Glyde, and S. T. Chui, *ibid.* **34**, 2815 (1986).
[28]H. Ma and S. T. Chui (private communication).
[29]L. K. Moleko and H. R. Glyde, Phys. Rev. B **30**, 4215 (1984).
[30]A. L. Fetter, P. C. Hohenberg, and P. Pincus, Phys. Rev. **147**, 140 (1966).
[31]V. V. Goldmann, J. Phys. Chem. Solids **30**, 1019 (1969).
[32]J. P. Hansen, Phys. Rev. A **2**, 221 (1970).
[33]H. R. Glyde and R. Taylor, Phys. Rev. B **5**, 1206 (1972).
[34]E. L. Pollock and J. P. Hansen, Phys. Rev. A **8**, 3110 (1973).
[35]H. R. Glyde and G. H. Keech, Ann. Phys. (N.Y.) **127**, 330 (1980).
[36]C. M. Fowler *et al.* (unpublished).
[37]E. H. Brandt, Int. J. Mod. Phys. B **5**, 751 (1991).
[38]A. Sudbø and E. H. Brandt, Phys. Rev. Lett. **66**, 1781 (1991).
[39]A. I. Larkin and Yu. N. Ovchinnikov, J. Low Temp. Phys. **43**, 409 (1979).
[40]M. V. Feigel'man and V. M. Vinokur, Phys. Rev. B **41**, 8986 (1990).
[41]P. H. Kes, J. Aarts, V. M. Vinokur, and C. J. Van der Beek, Phys. Rev. Lett. **64**, 1063 (1990).
[42]S. Chakravartes, B. I. Ivlev, and Yu. N. Ovchinnikov, Phys. Rev. B **42**, 2143 (1990).
[43]R. H. Koch, V. Foglietti, W. J. Gallagher, G. Koven, A. Gupta, and M.P.A. Fisher, Phys. Rev. Lett. **63**, 1511 (1989).
[44]T.T.M. Palstra, B. Battlogg, R. B. van Dover, L. F. Schneemeyer, and J. V. Waszczak, Phys. Rev. B **41**, 6621 (1990).
[45]L. Civale, T. K. Worthington, and A. Gupta, Phys. Rev. B **43**, 5425 (1991).